APPLYING CORRELATION METHODS TO RELATIVE NAVIGATION

Rachel Mamich[*], Renato Zanetti[†]

This study introduces an adaptive relative navigation filter, employing correlation methods to autonomously discern and estimate the impacts of unmodeled perturbations on a two spacecraft relative inertial system. These perturbations are due to differences in gravity models used in simulation truth and filter dynamics. This research demonstrates that the integration of adaptive strategies empowers the filter to dynamically accommodate unforeseen perturbations, facilitating estimation without assumptions regarding timing, optimality, or magnitude. The findings underscore the versatility of correlation methods, and their ability to handle the nonlinear dual inertial system presented.

INTRODUCTION

The Kalman Filter (KF)[1,2] operates under the assumption that models of the state space dynamics and measurements are known exactly. In practical aerospace systems, perfect knowledge of the models is not possible; additionally, unexpected events can alter the dynamics of the state or the way that a sensor is functioning. When the models become mismatched, it can lead to degraded estimation performance and even filter divergence.

In aerospace applications, spacecraft are limited in their computational power and thus the onboard dynamics models must be truncated to keep the system tractable. Onboard dynamics models are typically selected to balance computational burden with adjustments to the assumed level of noise in the system. Many of the common dynamics assumptions stem from environmental factors like the model of the central body that the orbit revolves around. These discrepancies are typically accounted for with extensive testing against a high fidelity model.

Adaptive estimation (or filtering) aims to estimate the state of the system while simultaneously reducing uncertainty in the model.[3,4] Adaptive filters can be broken down into a handful of major categories correlation methods,[3,5–11] covariance matching methods,[12–16] maximum likelihood methods,[17–19] Bayesian methods,[20–22] subspace methods,[23] and predictor error methods.[24] In this work, correlation methods are taken and applied to a relative navigation algorithm to enable autonomous, onboard maneuver estimation as well as onboard covariance estimation for two spacecraft in close proximity.

An algorithm is proposed to apply process noise adaptation via correlation methods to a relative navigation scenario. This algorithm is referred to as MILTON, or Measurement Innovation Leveraging To Obtain Noise. The intent of this paper is to demonstrate the viability of using MILTON to estimate an unknown level of process noise.

[*]NSTGRO Fellow and Graduate Student, Aerospace Engineering and Engineering Mechanics, University of Texas at Austin, 2617 Wichita St, Austin, TX 78712.

[†]Associate Professor, Aerospace Engineering and Engineering Mechanics, University of Texas at Austin, 2617 Wichita St, Austin, TX 78712.

The remainder of this paper is organized as follows: first, background information on the foundational concepts used to construct the algorithm presented. Next, the design of the navigation filter is covered. Then, the results from applying correlation methods to a scenario with a fixed level of process noise is presented. Finally, conclusions are drawn and future work is addressed.

BACKGROUND

The algorithm developed in this study, MILTON, consists of two primary components. This section offers an overview of these fundamental components.

The initial component of MILTON is the Extended Kalman Filter (EKF). The EKF is a widely utilized estimation algorithm in the aerospace industry, favored for its minimal computational demands. This computational ease stems from its use of first-order Taylor approximations.[25] These approximations are centered on the estimated 'nominal' state and thus the filter has the potential to diverge if the estimated 'nominal' state drifts too far from the truth. The EKF itself is broken up into two main parts: time propagation and measurement update. The EKF time propagation equations are,

$$\begin{aligned} &\dot{\mathbf{x}}_k = \mathbf{f}\left(\mathbf{x}_k^+, t\right), \quad \mathbf{P}_{k+1}^- = \mathbf{F}\mathbf{P}_k^+\mathbf{F}^T + \hat{\mathbf{Q}}, \\ &\mathbf{F} = \mathrm{e}^{\mathbf{A}\Delta t}, \qquad\quad \mathbf{A} = \left.\frac{\partial \mathbf{f}}{\partial \mathbf{x}}\right|_{\mathbf{x}_k^-}, \end{aligned} \tag{1}$$

where $\mathbf{x}$ is the state of size n, $\mathbf{f}()$ is the function that governs the state dynamics, t is time, $\mathbf{P}$ is the filter covariance estimate, $\mathbf{F}$ is the discrete time state transition matrix, and $\hat{\mathbf{Q}}$ is the discrete time process noise matrix. The superscript, $()^-$, indicates that the quantity is the prior estimate. The subscripts $()_k$ and $()_{k+1}$ indicate that the quantity is at time step k and $k+1$ respectively. The EKF measurement update equations are,

$$\begin{aligned} &\mathbf{x}_{k+1}^+ = \mathbf{x}_{k+1}^+ + \mathbf{K}\left(\mathbf{y}_{k+1} - \mathbf{h}\left(\mathbf{x}_{k+1}^-\right)\right), \quad \mathbf{K} = \mathbf{P}_{k+1}^-\mathbf{H}_{k+1}^T\left(\mathbf{H}_{k+1}\mathbf{P}_{k+1}^-\mathbf{H}_{k+1}^T + \mathbf{R}\right)^{-1}, \\ &\mathbf{P}_{k+1}^+ = \left(\mathbf{I} - \mathbf{K}\mathbf{H}_{k+1}\right)\mathbf{P}_{k+1}^-\left(\mathbf{I} - \mathbf{K}\mathbf{H}_{k+1}\right)^T + \mathbf{K}\mathbf{R}\mathbf{K}^T, \;\; \mathbf{H}_{k+1} = \left.\frac{\partial \mathbf{h}}{\partial \mathbf{x}}\right|_{\mathbf{x}_{k+1}^-}, \end{aligned} \tag{2}$$

where $\mathbf{K}$ is the Kalman gain, $\mathbf{I}$ is the identity matrix, $\mathbf{y}_{k+1}$ is the received measurement of size m, $\mathbf{h}()$ is the measurement function that relates the state to the measurement, $\mathbf{H}$ is the measurement Jacobian, $\mathbf{R}$ is the measurement noise, and the superscript, $()^+$, indicates that the quantity is the posterior estimate. In a traditional framework, the filter cycles through the propagation and measurement update steps until there are no more measurements and the estimated state and covariance matrices are returned.

The second component of MILTON, placed after the EKF measurement update and before the next EKF propagation, is the adaptation. The adaptive component runs correlation methods for process noise adaptation. In previous work on correlation methods, the theory has been applied to linear systems.[3,9,11] In this previous work, a time series of *linear* measurements is taken and used to construct the correlation method equations. From,[11]

$$\mathbf{C}_{k,k-p} = \mathbb{E}\left[\mathcal{Z}_k\mathcal{Z}_{k-p}^T\right] = \sum_{i=p+1}^{m_b}\mathbf{B}_i^k\hat{\mathbf{Q}}\mathbf{B}_{i-p}^{k-pT} + \sum_{i=p}^{m_b}\mathbf{A}_i^k\mathbf{R}\mathbf{A}_{i-p}^{k-pT}, \tag{3}$$

where $\mathbf{C}_{k,k-p}$ is the autocorrelation of time steps k and $k-p$ and $p \in [0, m_b]$. The quantities $\mathcal{Z}$, $\mathbf{A_i^k}$, and $\mathbf{B_i^k}$ are defined in.[11] Written differently in,[11]

$$\underbrace{\begin{bmatrix} \text{vech}\left(\hat{\mathbf{C}}_{k,k}\right) \\ \text{vec}\left(\hat{\mathbf{C}}_{k,k-1}\right) \\ \vdots \\ \text{vec}\left(\hat{\mathbf{C}}_{k,k-m_b}\right) \end{bmatrix}}_{\triangleq \mathbf{c}_k} = \underbrace{\begin{bmatrix} \sum_{i=1}^{m_b} \mathbf{B}_i^k \otimes_h \mathbf{B}_i^k & \sum_{i=0}^{m_b} \mathbf{A}_i^k \otimes_h \mathbf{A}_i^k \\ \sum_{i=2}^{m_b} \mathbf{B}_{i-1}^{k-1} \otimes_u \mathbf{B}_i^k & \sum_{i=1}^{m_b} \mathbf{A}_{i-1}^{k-1} \otimes_u \mathbf{A}_i^k \\ \vdots & \vdots \\ \sum_{i=m_b+1}^{m_b} \mathbf{B}_{i-m_b-1}^{k-m_b-1} \otimes_u \mathbf{B}_i^k & \sum_{i=m_b}^{m_b} \mathbf{A}_{i-m_b}^{k-m_b} \otimes_u \mathbf{A}_i^k \end{bmatrix}}_{\triangleq \mathbf{D}_k} \underbrace{\begin{bmatrix} \text{vech}\left(\hat{\mathbf{Q}}\right) \\ \text{vech}\left(\mathbf{R}\right) \end{bmatrix}}_{\triangleq \boldsymbol{\theta}_k}, \quad (4)$$

where $\hat{C}$ is the 'measured' autocorrelation, and vech() and vec() are defined as,

$$\mathbf{R} = \begin{bmatrix} r_{11} & r_{12} & r_{13} \\ r_{21} & r_{22} & r_{23} \\ r_{31} & r_{32} & r_{33} \end{bmatrix}, \quad \begin{matrix} \text{vec}\left(\mathbf{R}\right) = \begin{bmatrix} r_{11} & r_{12} & r_{13} & r_{21} & r_{22} & r_{23} & r_{31} & r_{32} & r_{33} \end{bmatrix}^T \\ \text{vech}\left(\mathbf{R}\right) = \begin{bmatrix} r_{11} & r_{12} & r_{13} & r_{22} & r_{23} & r_{33} \end{bmatrix}^T \end{matrix}, \quad (5)$$

and $\otimes$ represents a Kroneker product with the known property $\text{vec}\left(\mathbf{AXB}\right) = \left(\mathbf{B}^T \otimes \mathbf{A}\right) \text{vec}(\mathbf{X})$. With single sided symmetry, a special Kroneker product relationship is defined as $\text{vec}\left(\mathbf{AXB}\right) = \left(\mathbf{B}^T \otimes_u \mathbf{A}\right) \text{vech}(\mathbf{X})$. With two-sided symmetry, this relathionship can be written as $\text{vech}\left(\mathbf{AXA^T}\right) = \left(\mathbf{A} \otimes_h \mathbf{A}\right) \text{vech}(\mathbf{X})$. In ,[11] (4) is used as a 'measurement model' in a recursive least squares framework with initial estimate and uncertainty $(\hat{\boldsymbol{\theta}}_0, \boldsymbol{\Psi}_0)$.

Examining (4) reveals that while the estimation of the upper triangular entries of the noise matrices guarantees symmetry, it does not ensure positive definiteness. For the covariance matrix of the state estimate to remain positive definite, the process noise matrix must also be positive definite. Early studies address this challenge heuristically; they opt simply to not update the estimate when positive definiteness is compromised.[3,26] More recently, [11] approaches this issue by using Riemann manifolds to estimate the noise matrices for linear systems. While this method effectively ensures positive definiteness, it is computationally demanding, posing significant challenges for deployment on spacecraft.

NAVIGATION DESIGN

This section covers the design of the relative navigation filter, MILTON. The state space is comprised of the relative inertial target position and velocity, the target vehicle's unmodeled acceleration in the inertial frame, the inertial chaser position and velocity, and accelerometer bias terms in the body frame for the chaser vehicle. The state space is,

$$\mathbf{X} = \begin{bmatrix} (\mathbf{r}_{t/c}^N)^T & (\mathbf{v}_{t/c}^N)^T & (\mathbf{a}_t^N)^T & (\mathbf{r}_c^N)^T & (\mathbf{v}_c^N)^T & (\mathbf{b}_c^{B_c})^T \end{bmatrix}^T, \quad (6)$$

where $\mathbf{r}$ indicates a position vector, $\mathbf{v}$ indicates a velocity vector, $\mathbf{a}$ indicates an acceleration vector, and $\mathbf{b}$ represents an acceleration bias vector. In this work, the superscript ^{N} indicates that the vector is represented in the inertial frame and the superscripts ^{B_t} and ^{B_c} indicate that the vectors are represented in the target body frame and the chaser body frame respectively. Lastly, when a vector has a subscript of the form $_{t/c}$ it indicates that the vector is from the chaser to the target vehicle and when the subscript is a single letter like $_c$ it indicates that the origin of the vector is the origin of

the frame it is represented in and ends at the subscript. In the research outlined in this document, it is unnecessary to incorporate an unmodeled target vehicle acceleration or a chaser accelerometer bias term. However, these elements are included to facilitate the consideration of deterministic perturbations in future studies. By incorporating these factors, this study demonstrates that the filter operates effectively under more 'nominal' conditions and retains the capacity to handle more complex scenarios. Including both of these additional states is crucial to prevent the bias in the chaser's accelerometer from being mistakenly attributed to an unmodeled target acceleration. Now that the state space is established, the details of the main components of the filter are detailed below.

Propagation

In the propagation phase, each spacecraft state is propagated independently using a fixed step Runge-Kutta (RK4) propagator. This means that the relative inertial states of the target are converted to the full inertial representation prior to propagation and are converted back after. This conversion is done by,

$$\mathbf{r}_{t/c}^N = \mathbf{r}_t^N - \mathbf{r}_c^N, \quad \mathbf{v}_{t/c}^N = \mathbf{v}_t^N - \mathbf{v}_c^N m. \tag{7}$$

Once the conversion to the full inertial state is done, the states are propagated with,

$$\mathbf{f}(\mathbf{X}) = \dot{\mathbf{X}} = \begin{bmatrix} \dot{\mathbf{r}}_t^N \\ \dot{\mathbf{v}}_t^N \\ \dot{\mathbf{a}}_t^N \\ \dot{\mathbf{r}}_c^N \\ \dot{\mathbf{v}}_c^N \\ \dot{\mathbf{b}}_c^{B_c} \end{bmatrix} = \begin{bmatrix} \mathbf{v}_t^N \\ \mathbf{g}_t^N + \mathbf{a}_t^N \\ \boldsymbol{\nu}_t \\ \mathbf{v}_c^N \\ \mathbf{g}_t^N + \mathbf{NB_c}\left(\boldsymbol{\alpha}_c^{B_c} - \mathbf{b}_c^{B_c}\right) + \boldsymbol{\nu}_c \Delta t \\ -\beta \mathbf{b}^{B_c} \end{bmatrix}, \tag{8}$$

where $\mathbf{g}$ is the acceleration of the spacecraft due to the central body's gravitational field, $\mathbf{NB_c}$ is the direction cosine matrix (DCM) from the chaser body frame to the inertial frame, $\boldsymbol{\alpha}_c$ is the measured acceleration from the chaser's onboard accelerometer, and β is the time constant for the Markov process of the accelerometer bias. The acceleration, velocity, and position are directly related through kinematics. The acceleration terms are governed primarily by Earth's gravity. Since the acceleration on the target is unknown, it is assumed that the acceleration term is constant over each time step. It should be noted that while the noise term $\boldsymbol{\nu}_t$ appears in (8), there is no artificial noise added to either the true propagation or the filter propagation. This term serves as a placeholder for the assumed form the process noise adaptation expects model discrepancies to take.

There are two separate gravity models used in the simulation: one to generate the true spacecraft state, one to propagate the estimated state in the filter itself. The gravity model used to propagate the true state includes two body dynamics with $J_2 - J_6$ zonal harmonic perturbations. While the gravity model used in the filter propagation includes two body dynamics with $J_2 - J_4$ only,

$$\begin{aligned} \mathbf{a}_{\text{truth}} &= \mathbf{a}_{\text{TBP}} + \sum_{i=2}^{6} \mathbf{a}_i, \\ \mathbf{a}_{\text{filter}} &= \mathbf{a}_{\text{TBP}} + \sum_{i=2}^{4} \mathbf{a}_i. \end{aligned} \tag{9}$$

Both of these models are derived using the Legendre polynomials and the gravity potential from.[27] For clarity, the target vehicle and chaser vehicle are both propagated with the $\mathbf{a}_{\text{truth}}$ gravity model in

truth generation and are both propagated with $\mathbf{a}_{\text{filter}}$ in the filter. As mentioned previously, there is a limit to the complexity of the dynamics model that a spacecraft can implement onboard and thus there is always a degree of model discrepancy between the truth and the modeled dynamics. Two separate gravity models are used here to emulate this difference in a scaled down fashion.

Maneuvers performed by the chaser are expected to be captured by the onboard accelerometer. Thus these accelerations are modeled as measurements from the accelerometer held constant over each propagation step. As previously mentioned, the bias term is necessary to avoid attributing sensor bias in the chaser to unmodeled accelerations in the target vehicle. Sensors often have bias values that vary over the length of a mission. This variability is often modeled as a Gauss-Markov process thus this study models its accelerometer bias as a Gauss-Markov process.

It should be noted that the accelerometer measurements are not always used directly in the propagation of the chaser vehicle. When the magnitude of the accelerometer reading is below a gating threshold, the measurements are not used in propagation, but instead are treated as direct measurements of the accelerometer bias terms.[28] This will be explained in more detail in the following section.

The covariance is propagated using the EKF propagation (1) constructing $\mathbf{A}$ using the following,

$$\mathbf{A} = \begin{bmatrix} \mathbf{A}_t & \mathbf{A}_{t/c} \\ \mathbf{0}_{9\times 9} & \mathbf{A}_c \end{bmatrix} \text{where,} \quad \mathbf{A}_{t/c} = \begin{bmatrix} \mathbf{0}_{3\times 3} & \mathbf{0}_{3\times 3} & \mathbf{0}_{3\times 3} \\ \frac{\partial \mathbf{g}_t}{\partial \mathbf{r}_t} - \frac{\partial \mathbf{g}_c}{\partial \mathbf{r}_c} & \mathbf{0}_{3\times 3} & \mathbf{N}\mathbf{B}_c \\ \mathbf{0}_{3\times 3} & \mathbf{0}_{3\times 3} & \mathbf{0}_{3\times 3} \end{bmatrix}, \tag{10}$$

where $\mathbf{A}_t$ and $\mathbf{A}_c$ are the Jacobians of the dynamics of the target and chaser vehicles with respect to their states.

In the filter, he process noise on the relative target vehicle states is assumed to be applied as a random jerk sampled from a normal distribution with zero mean and a covariance of $\mathbf{Q}$, the continuous time process noise matrix. This is done independently for the target vehicle and the chaser vehicle respectively. Thus the relationship between the continuous time process noise and the discrete time process noise is,

$$\hat{\mathbf{Q}} = \begin{bmatrix} \frac{\Delta t^5}{36}\mathbf{Q} & \frac{\Delta t^4}{12}\mathbf{Q} & \frac{\Delta t^3}{6}\mathbf{Q} \\ \frac{\Delta t^4}{12}\mathbf{Q} & \frac{\Delta t^3}{4}\mathbf{Q} & \frac{\Delta t^2}{2}\mathbf{Q} \\ \frac{\Delta t^3}{6}\mathbf{Q} & \frac{\Delta t^2}{2}\mathbf{Q} & \Delta t\mathbf{Q} \end{bmatrix}. \tag{11}$$

As seen in (1), the filter itself neglects the process noise when propagating the state itself, so the term $\boldsymbol{\nu}_t$ is zeroed out in the filter.

Measurement Update

The EKF measurement update uses relative range and bearing measurements taken from the chaser to the target vehicle. It is assumed that the range and bearing measurements are provided by a scanning LiDAR. The relative range is calculated as,

$$\rho = \left| \mathbf{r}_{t/c}^{L_c} \right|. \tag{12}$$

The relative bearing measurements are assumed to be in the center of the LiDAR frame. The relative azimuth and elevation angles are calculated using,

$$\begin{aligned} A &= \arctan\left(\frac{\rho_x}{\rho_z}\right), \\ B &= \arctan\left(\frac{\rho_y}{\rho_z}\right), \end{aligned} \tag{13}$$

where $\boldsymbol{\rho}$ is the unit vector defined in the LiDAR frame that defines the relative position of the target with respect to the chaser vehicle. $\boldsymbol{\rho}$ can be found using,

$$\boldsymbol{\rho} = \mathbf{L}_c\mathbf{N}\left(\frac{\mathbf{r}_{t/c}}{|\mathbf{r}_{t/c}|}\right), \tag{14}$$

where $\mathbf{L}_c\mathbf{N}$ is the DCM from the inertial frame to the chaser LiDAR frame.

As previously mentioned, when the magnitude of the measurement taken by the accelerometer is below a gating threshold, the accelerometer measurement is taken to be a direct measurement of the accelerometer bias,[28]

$$\mathbf{b}_c = \boldsymbol{\alpha}_c. \tag{15}$$

Thus the measurement Jacobian takes one of two forms during the measurement update:

$$\mathbf{H} = \begin{bmatrix} \frac{1}{\rho}\mathbf{r}_{t/c}\mathbf{I}_{3\times3} & \mathbf{0}_{3\times15} \end{bmatrix} \quad \text{or} \quad \mathbf{H} = \begin{bmatrix} \frac{1}{\rho}\mathbf{r}_{t/c}\mathbf{I}_{3\times3} & \mathbf{0}_{3\times15} \\ \mathbf{0}_{3\times15} & \mathbf{I}_{3\times3} \end{bmatrix}. \tag{16}$$

By constructing the observability matrix the full system is determined to be observable.[29] However, none of the measurements used in this system are inertial. This means that while the chaser elements are technically observable there is no additional inertial information coming into the system, and thus updating the full inertial state can adversely impact the filter's performance. Consequently, the chaser's position and velocity are treated as consider parameters.[25] This adjustment involves modifying the Kalman gain derived in (2), specifically by setting the values in the rows corresponding to the chaser's position and velocity to zero:

$$K[10:15,:] = 0. \tag{17}$$

Process Noise Adaptation

In this study, correlation methods are employed to facilitate process noise adaptation for the relative target vehicle states. The background section reviews prior research on correlation methods, noting that earlier investigations predominantly focused on *linear* systems. In contrast, the system addressed in this work is *nonlinear*; however, the measurement residuals are presumed to be linear relative to the state errors. The measurement residuals can be organized into a time series and vectorized as follows:

$$\underbrace{\begin{bmatrix}\mathbf{r}_k\\ \mathbf{r}_{k-1}\\ \vdots\\ \mathbf{r}_{k-m_b+1}\end{bmatrix}}_{\triangleq \mathcal{Y}_{k,k-m_b+1}} = \underbrace{\begin{bmatrix}\mathbf{H}_k\mathbf{\Phi}_{k,k-m_b+1}\\ \mathbf{H}_{k-1}\mathbf{\Phi}_{k-1,k-m_b+1}\\ \vdots\\ \mathbf{H}_{k-m_b+1}\end{bmatrix}}_{\triangleq \mathcal{O}_{k,k-m_b+1}} \mathbf{e}_{k-m_b+1}$$
$$+ \underbrace{\begin{bmatrix}\mathbf{H}_k & \mathbf{H}_k\mathbf{F}_{k-1} & \mathbf{H}_k\mathbf{\Phi}_{k,k-2} & \cdots & \mathbf{H}_k\mathbf{\Phi}_{k,k-m_b+2}\\ \mathbf{0}_{m\times n} & \mathbf{H}_{k-1} & \mathbf{H}_{k-1}\mathbf{F}_{k-2} & \cdots & \mathbf{H}_{k-1}\mathbf{\Phi}_{k-1,k-m_b+2}\\ \vdots & \vdots & \ddots & \vdots & \vdots\\ \mathbf{0}_{m\times n} & \mathbf{0}_{m\times n} & \mathbf{0}_{m\times n} & \mathbf{0}_{m\times n} & \mathbf{H}_{k-m_b+2}\\ \mathbf{0}_{m\times n} & \mathbf{0}_{m\times n} & \mathbf{0}_{m\times n} & \mathbf{0}_{m\times n} & \mathbf{0}_{m\times n}\end{bmatrix}}_{\triangleq \mathcal{M}^w_{k-1,k-m_b+1}} \underbrace{\begin{bmatrix}\boldsymbol{\nu}_{k-1}\\ \boldsymbol{\nu}_{k-2}\\ \vdots\\ \boldsymbol{\nu}_{k-m_b+1}\end{bmatrix}}_{\triangleq \mathcal{V}_{k-1,k-m_b+1}} + \underbrace{\begin{bmatrix}\boldsymbol{\eta}_k\\ \boldsymbol{\eta}_{k-1}\\ \vdots\\ \boldsymbol{\eta}_{k-m_b+1}\end{bmatrix}}_{\triangleq \mathcal{W}_{k,k-m_b+1}}. \tag{18}$$

where m_b is the buffer size, $\mathbf{r}_k$ is the measurement residual at time k, $\mathbf{e}_k$ is the state error at time k, $\mathbf{\Phi}_{k,k-m_b+1}$ is the discrete time state transition matrix from time step $k-m_b+1$ to k and $\boldsymbol{\nu}_k$ and $\boldsymbol{\eta}_k$ are random samples from the discrete time process noise and measurement noise respectively. Shown more compactly:

$$\mathcal{Y}_{k,k-m_b+1} = \mathcal{O}_{k,k-m_b+1}\mathbf{e}_{k-m_b+1} + \mathcal{M}^w_{k-1,k-m_b+1}\mathcal{V}_{k-1,k-m_b+1} + \mathcal{W}_{k,k-m_b+1}. \tag{19}$$

It is important to note that the derivation presented in this document is included for completeness. With the assumption that the measurement residuals are linear in relation to the state errors, the derivation adheres to the methodology outlined in.[11] However, it is worth mentioning that the matrices involved are Jacobians of nonlinear functions, evaluated based on the most recent state estimate.

To isolate the state *error* vector, multiply both sides by $\mathcal{O}^T_{k,k-m_b+1}$ yielding:

$$\begin{aligned}\mathcal{O}^T_{k,k-m_b+1}\mathcal{Y}_{k,k-m_b+1} = \mathcal{M}_{k,k-m_b+1}\mathbf{e}_{k-m_b+1} &+ \mathcal{O}^T_{k,k-m_b+1}\mathcal{M}^w_{k-1,k-m_b+1}\mathcal{V}_{k-1,k-m_b+1}\\ &+ \mathcal{O}^T_{k,k-m_b+1}\mathcal{W}_{k,k-m_b+1}.\end{aligned} \tag{20}$$

where $\mathcal{M}_{k,k-m_b+1}$ is the observability Gramian from time step $k-m_b+1$ to k. In this work, it is assumed that the observability Gramian is invertable. This is a reasonable assumption to make in this work because the adaptation is being applied only to the target vehicle states. As discussed in the measurement update section, the relative target states are fully observable. To isolate the state *errors*, multiply both sides of (20) by $\mathcal{M}^{-1}_{k,k-m_b+1}$:

$$\begin{aligned}\mathcal{M}^{-1}_{k,k-m_b+1}\mathcal{O}^T_{k,k-m_b+1}\mathcal{Y}_{k,k-m_b+1} = \mathbf{e}_{k-m_b+1} &+ \mathcal{M}^{-1}_{k,k-m_b+1}\mathcal{O}^T_{k,k-m_b+1}\mathcal{M}^w_{k-1,k-m_b+1}\mathcal{V}_{k-1,k-m_b+1}\\ &+ \mathcal{M}^{-1}_{k,k-m_b+1}\mathcal{O}^T_{k,k-m_b+1}\mathcal{W}_{k,k-m_b+1}.\end{aligned} \tag{21}$$

Suppose this vectorization is repeated for measurements taken from time step $k - m_b$ to $k - 1$.

$$\begin{aligned}\mathcal{M}_{k,k-m_b+1}^{-1}\mathcal{O}_{k,k-m_b+1}^{T}\mathcal{Y}_{k,k-m_b+1} &= \mathbf{e}_{k-m_b+1}+\mathcal{M}_{k,k-m_b+1}^{-1}\mathcal{O}_{k,k-m_b+1}^{T}\mathcal{M}_{k-1,k-m_b+1}^{w}\mathcal{V}_{k-1,k-m_b+1}\\ &\quad+\mathcal{M}_{k,k-m_b+1}^{-1}\mathcal{O}_{k,k-m_b+1}^{T}\mathcal{W}_{k,k-m_b+1},\\ \mathcal{M}_{k-1,k-m_b}^{-1}\mathcal{O}_{k-1,k-m_b}^{T}\mathcal{Y}_{k-1,k-m_b} &= \mathbf{e}_{k-m_b}+\mathcal{M}_{k-1,k-m_b}^{-1}\mathcal{O}_{k-1,k-m_b}^{T}\mathcal{M}_{k-2,k-m_b}^{w}\mathcal{V}_{k-2,k-m_b}\\ &\quad+\mathcal{M}_{k-1,k-m_b}^{-1}\mathcal{O}_{k-1,k-m_b}^{T}\mathcal{W}_{k-1,k-m_b}.\end{aligned} \tag{22}$$

Now substitute $\mathbf{e}_{k-m_b+1} = \mathbf{F}_{k-m_b}\mathbf{e}_{k-m_b} + \boldsymbol{\nu}_{k-m_b}$ and subtract one equation from the other:

$$\mathcal{Z}_k = \mathcal{A}_k\mathcal{Y}_{k,k-m_b} = \mathcal{B}_k\mathcal{V}_{k-1,k-m_b} + \mathcal{B}_k\mathcal{W}_{k,k-m_b}, \tag{23}$$

where $\mathcal{A}_k$ is defined as:

$$\mathcal{A}_k = \left[\mathcal{M}_{k,k-m_b+1}^{-1}\mathcal{O}_{k,k-m_b+1}^{T}, \mathbf{0}_{n\times m}\right] - \left[\mathbf{0}_{n\times m}, \mathbf{F}_{k-m_b}\mathcal{M}_{k-1,k-m_b}^{-1}\mathcal{O}_{k-1,k-m_b}^{T}\right], \tag{24}$$

and $\mathcal{B}_k$ is defined as:

$$\begin{aligned}\mathcal{B}_k = &\left[\mathcal{M}_{k,k-m_b+1}^{-1}\mathcal{O}_{k,k-m_b+1}^{T}\mathcal{M}_{k-1,k-m_b+1}^{w}, \mathbf{I}_{n\times n}\right]\\ &- \left[\mathbf{0}_{n\times n}, \mathbf{F}_{k-m_b}\mathcal{M}_{k-1,k-m_b}^{-1}\mathcal{O}_{k-1,k-m_b}^{T}\mathcal{M}_{k-2,k-m_b}^{w}\right],\end{aligned} \tag{25}$$

again, the definitions in (24) and (25) are identical to the quantities for a linear system in .[11]

The 'measurement' of the autocorrelation is generated by using the measurement residuals and their relationship to $\mathcal{Z}_k$ outlined in (23) and applying the relationship in (3) as $\hat{\mathbf{C}}_{k,k-p} = \hat{\mathcal{Z}}\hat{\mathcal{Z}}^T$.

This is where the work presented in this paper begins to diverge again from the previous work. In previous work the process noise matrix is guaranteed to be symmetric. The positive definiteness however is not. In much of the work on correlation methods, the positive definiteness is guaranteed by simply not updating the process noise if positive definiteness is violated .[3,26] In [11] this issue is treated by applying Riemann manifolds, however this solution is computationally expensive. Here, correlation methods are applied to the specific nonlinear problem of relative navigation which allows for strategic choices to be made.

While prior research ensures the symmetry of the process noise matrix, its positive definiteness is often not guaranteed. Commonly, in correlation method studies, positive definiteness is maintained by refraining from updating the process noise if this condition is compromised.[3,26] In[11] this issue is addressed by using Riemann manifolds, though this approach is computationally intensive.[11] In contrast, this work applies correlation methods to the specific nonlinear problem of relative navigation, facilitating strategic decisions for the given problem.

It is assumed that the process noise acts as a jerk term where the continuous time process noise and the discrete time process noise are related via (11). So far, these assumptions ensure symmetry, but not positive definiteness. Another common assumption is that the continuous time process noise matrix is a diagonal matrix .[30,31] To ensure positive definiteness, MILTON estimates the component-wise square root of the diagonal of the continuous time process noise matrix. Additionally, to keep the focus of this work on process noise estimation, the measurement noise is assumed to be known. This alters (4) and yields:

$$
\begin{aligned}
\hat{\mathbf{c}}_k &= \hat{\mathbf{D}}_k \mathbf{s}_k, \\
\hat{\mathbf{c}}_k &= \begin{bmatrix} \text{vech}\left(\hat{\mathbf{C}}_{k,k}\right) \\ \text{vec}\left(\hat{\mathbf{C}}_{k,k-1}\right) \\ \vdots \\ \text{vec}\left(\hat{\mathbf{C}}_{k,k-m_b}\right) \end{bmatrix} - \begin{bmatrix} \sum_{i=0}^{m_b} \mathbf{A}_i^k \otimes_h \mathbf{A}_i^{kT} \\ \sum_{i=1}^{m_b} \mathbf{A}_{i-1}^{k-1} \otimes_u \mathbf{A}_i^{kT} \\ \vdots \\ \sum_{i=m_b}^{m_b} \mathbf{A}_{i-m_b}^{k-m_b} \otimes_u \mathbf{A}_i^{kT} \end{bmatrix} \text{vech}\left(\mathbf{R}\right), \\
\hat{\mathbf{D}}_k &= \begin{bmatrix} \sum_{i=1}^{m_b} \mathbf{B}_i^k \otimes_h \mathbf{B}_i^{kT} \\ \sum_{i=2}^{m_b} \mathbf{B}_{i-1}^{k-1} \otimes_u \mathbf{B}_i^{kT} \\ \vdots \\ \sum_{i=m_b+1}^{m_b} \mathbf{B}_{i-m_b-1}^{k-m_b-1} \otimes_u \mathbf{B}_i^{kT} \end{bmatrix} [\mathbf{D}_{\text{vech}} \mathbf{s}_k] \frac{\partial \mathbf{Q}_{\text{diag}}}{\partial \mathbf{s}_k},
\end{aligned}
\tag{26}
$$

where $\mathbf{s}_k$ is the square root of the continuous time process noise matrix diagonal, $[\mathbf{D}_{\text{vech}}\mathbf{s}_k]$ is the matrix that transforms the continuous time process noise matrix diagonal to the upper triangular of the discrete time process noise matrix, and $\frac{\partial \mathbf{Q}_{\text{diag}}}{\partial \mathbf{s}_k}$ is the derivative of the continuous time process noise diagonal with respect to the square root of that diagonal. With this new 'measurement model' for the adaptation, *both* symmetry and positive definiteness are guaranteed.

Now examining (26), in traditional recursive least squares for this system, one must invert a matrix of size $m_b n^2 + \frac{(n+1)n}{2} \times m_b n^2 + \frac{(n+1)n}{2}$. In the work presented here, $n = 9$ and m_b can vary. Thus this inversion would minimally be 126×126 for a buffer size of $m_b = 1$. Clearly, this inversion poses a significant computational burden. By converting the recursive least squares to an information form allows for the largest inversion to be the size of $\mathbf{\Psi}$, or in terms of this system a 3×3. The equations that govern the information form are as follows :[25]

$$
\begin{aligned}
\mathbf{\Lambda}_k^+ &= \left(\mathbf{\Psi}_k^+\right)^{-1} \quad \mathbf{d}_k^+ = \mathbf{\Lambda}_k^+ \mathbf{s}_k^+, \\
\mathbf{\Lambda}_{k+1}^- &= \left(\mathbf{I}_{3\times 3} - \mathbf{\Lambda}_k^+ \left(\mathbf{\Lambda}_k^+ + \mathbf{Q}_w^{-1}\right)^{-1}\right) \mathbf{\Lambda}_k^+, \\
\mathbf{d}_{k+1}^- &= \left(\mathbf{I}_{3\times 3} - \mathbf{\Lambda}_k^+ \left(\mathbf{\Lambda}_k^+ + \mathbf{Q}_w^{-1}\right)^{-1}\right) \mathbf{d}_k^+, \\
\mathbf{d}_{k+1}^+ &= \mathbf{d}_{k+1}^- + \mathbf{D}_{k+1}^T \mathbf{R}_w^{-1} \mathbf{c}_{k+1}, \\
\mathbf{\Lambda}_{k+1}^+ &= \mathbf{\Lambda}_{k+1}^- + \mathbf{D}_{k+1}^T \mathbf{R}_w^{-1} \mathbf{D}_{k+1},
\end{aligned}
\tag{27}
$$

where $\mathbf{d}$ is the information state, $\mathbf{\Lambda}$ is the information matrix, and $\mathbf{Q}_w$ and $\mathbf{R}_w$ are the process noise and measurement noise for the adaptation itself. In this work, the adaptation process noise and measurement noise are assumed to be constant and thus their inversions can be calculated once offline. An important implementation note is that the information update is not run every time step, but instead is only called when the buffer of measurements, $\hat{\mathbf{c}}_k$ is full of completely new measurements, or once every $m_b + 1$ time steps. With the changes detailed in this section, this algorithm is capable of guaranteeing a positive definite process noise matrix for the nonlinear scenario of relative navigation with full relative state observability.

NUMERICAL RESULTS

This section covers the numerical results for a simulation beginning with two spacecraft in a string of pearls orbit with a constant level of process noise applied to the target vehicle. There are

no deterministic maneuvers performed to demonstrate MILTON's ability to estimate pure process noise.

The initial Keplerian elements for each spacecraft are shown below: The spacecraft are in Earth

Table 1: Initial Keplerian elements for the process noise only scenario.

Element	$a[m]$	$e[-]$	$inc[^\circ]$	$\Omega[^\circ]$	$\omega[^\circ]$	$M_0[^\circ]$
Target	6.878e6	0.0	95	0	0	2.8648e-4
Chaser	6.878e6	0.0	95	0	0	0

orbits with gravitational parameters listed below:

Table 2: Earth constants used in propagation.

Parameter	μ $\left[\frac{m^3}{s^2}\right]$	$J_2[-]$	$R_{Earth}[m]$
Value	3.986e14	.0010826269	6.378e6

The filter initial uncertainty used in each scenario is set to be:

$$\mathbf{P}_0 = \begin{bmatrix} 2\left(\frac{25}{3}\right)^2\mathbf{I}_{3\times3} & \mathbf{0}_{3\times3} & \mathbf{0}_{3\times3} & \left(\frac{25}{3}\right)^2\mathbf{I}_{3\times3} & \mathbf{0}_{3\times3} & \mathbf{0}_{3\times3} \\ \mathbf{0}_{3\times3} & 2\left(\frac{1}{10}\right)^2\mathbf{I}_{3\times3} & \mathbf{0}_{3\times3} & \mathbf{0}_{3\times3} & \left(\frac{1}{10}\right)^2\mathbf{I}_{3\times3} & \mathbf{0}_{3\times3} \\ \mathbf{0}_{3\times3} & \mathbf{0}_{3\times3} & (\text{1e-6})^2\mathbf{I}_{3\times3} & \mathbf{0}_{3\times3} & \mathbf{0}_{3\times3} & \mathbf{0}_{3\times3} \\ \left(\frac{25}{3}\right)^2\mathbf{I}_{3\times3} & \mathbf{0}_{3\times3} & \mathbf{0}_{3\times3} & \left(\frac{25}{3}\right)^2\mathbf{I}_{3\times3} & \mathbf{0}_{3\times3} & \mathbf{0}_{3\times3} \\ \mathbf{0}_{3\times3} & \left(\frac{1}{10}\right)^2\mathbf{I}_{3\times3} & \mathbf{0}_{3\times3} & \mathbf{0}_{3\times3} & \left(\frac{1}{10}\right)^2\mathbf{I}_{3\times3} & \mathbf{0}_{3\times3} \\ \mathbf{0}_{3\times3} & \mathbf{0}_{3\times3} & \mathbf{0}_{3\times3} & \mathbf{0}_{3\times3} & \mathbf{0}_{3\times3} & (\text{1e-6})^2\mathbf{I}_{3\times3} \end{bmatrix}, \tag{28}$$

where the position, velocity, and acceleration are in the units $m, m/s,$ andm/s^2. The initial uncertainty reflects that the vehicles have just lost GPS just prior to the scenario start. The simulation length is approximately 3500s.

LiDAR and accelerometer measurements are received every second. It is assumed that the LiDAR is oriented such that its field of view (FOV) is centered on the target vehicle. The accelerometer gating threshold is set to be 1e-4 and the accelerometer bias time constant is set to be $\beta = \frac{1}{3600}\frac{1}{s}$ with an initial bias of 2.9430e-05 $\frac{m}{s^2}$ for each axis. The measurement noise used in this scenario is:

$$\mathbf{R} = \begin{bmatrix} (0.01m)^2 & 0 & 0 & 0 \\ 0 & (0.1^\circ)^2 & 0 & 0 \\ 0 & 0 & (0.1^\circ)^2 & 0 \\ 0 & 0 & 0 & (3.433e-6m/s^2/\sqrt{s})^2 \end{bmatrix}, \tag{29}$$

the values in the top 3×3 reflect a combination of the uncertainty and bias terms shown in [32] for the RVS 3000-X LiDAR from Jena Optronik. The last value in the bottom right reflects the velocity random walk of the accelerometer used.

The adaptation buffer is set to be $m_b = 30$ and the adaptation process noise and measurement noise are set to be $\mathbf{Q}_w =$ 1e-5$\mathbf{I}_{3\times3}$ and $\mathbf{R}_w =$ 1e-1$\mathbf{I}$. The adaptation is initialized by sampling from a normal distribution centered on the true process noise with an uncertainty of $\mathbf{\Psi}_0 =$ 1e-6$\mathbf{I}_{3\times3}$.

A Monte Carlo study with 100 ($N_{\text{MC}} = 100$) runs is conducted and the results are shown below. In this study there are 100 truth trajectories created due to the need to randomize the process noise samples applied as jerks for each run. Each truth trajectory begins at the same initial state described by the Keplerian elements in Table 1. The filter in each run is initialized by randomly sampling from a normal distribution centered on the true initial state with an initial process noise matrix shown in (28). The results are presented in the RTN frame. The RTN frame is the radial, transverse, normal frame. It is defined such that the radial direction is in line with the inertial position vector, the normal is defined in the direction of the orbit normal, and the transverse completed the triad .[27]

Figures 1-6 show the results from the Monte Carlo analysis in the process noise only scenario. In each state error figure (1-4) there are four line styles. The Avg Err$^+$ line is the mean error across Monte Carlo runs at each time step, k,

$$\bar{\mathbf{e}}_k^+ = \frac{1}{N_{\text{MC}}} \sum_{i=1}^{N_{\text{MC}}} \mathbf{e}_k^{i+} = \frac{1}{N_{\text{MC}}} \sum_{i=1}^{N_{\text{MC}}} (\mathbf{x}_k^{i+} - \mathbf{x}_k^i), \tag{30}$$

where $\mathbf{x}_k^{i+}$ is the posterior estimated state from the ith Monte Carlo run at time step k and $\mathbf{x}_k^i$ is the truth state from the ith Monte Carlo run at time step k. The Error$^+$ lines show the error from each of the 100 Monte Carlo runs. The Avg $3\sigma^+$ shows the average 3σ bounds outputted from each Monte Carlo run from the EKF:

$$\bar{\mathbf{P}}_k^{EKF+} = \frac{1}{N_{\text{MC}}} \sum_{i=1}^{N_{\text{MC}}} \mathbf{P}_k^{EKF,i+}, \tag{31}$$

where $\mathbf{P}_k^{EKF,i+}$ is the estimated covariance matrix of the ith Monte Carlo run at time step k. The Sample $3\sigma^+$ reflects the sample 3σ bounds calculated using all 100 Monte Carlo runs:

$$\bar{\mathbf{P}}_k^+ = \frac{1}{N_{\text{MC}}} \sum_{i=1}^{N_{\text{MC}}} (\mathbf{e}_k^{i+} - \bar{\mathbf{e}}_k^{i+})(\mathbf{e}_k^{i+} - \bar{\mathbf{e}}_k^{i+})^T, \tag{32}$$

To evaluate whether the adaptation is functioning effectively, several key indicators should be examined. Firstly, the average error line should be approximately zero throughout the scenario, indicating that the filter is producing unbiased results. Secondly, the individual Monte Carlo simulations should largely fall within the average estimated 3σ bounds set by EKF. Lastly, there should be a close match between the average estimated 3σ bounds from the EKF and the sample 3σ.

It should be noted that the state error plots for the chaser vehicle are not included, as these states are treated as consider parameters and are not updated. Additionally, the initial 300 seconds of the results, where the filter error rapidly decreases, are omitted to provide better resolution in the latter portion of the scenario.

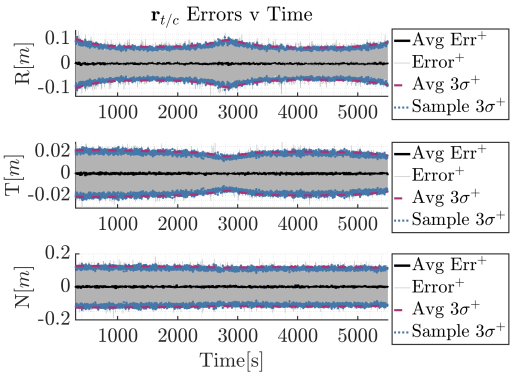

Figure 1: Relative position of the target vehicle errors in the target RTN frame versus time excluding initial 300s.

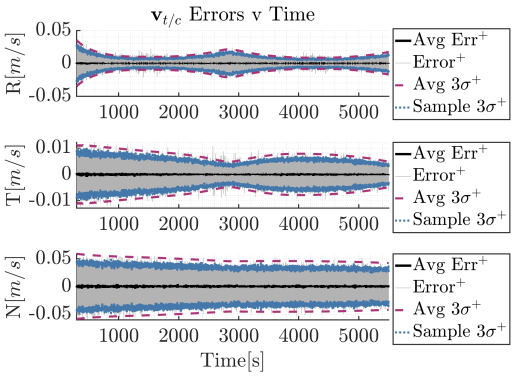

Figure 2: Relative velocity of the target vehicle errors in the target RTN frame versus time excluding initial 300s.

It is clear that the adaptation successfully approximates the true process noise in the system by examining the average $3\sigma^+$ bounds compared with the sample 3σ bounds in Figure 1. While the estimated bounds in Figures 2 and 3 overestimate the errors in the relative velocity and acceleration, the bounds for the relative position are nearly perfect.

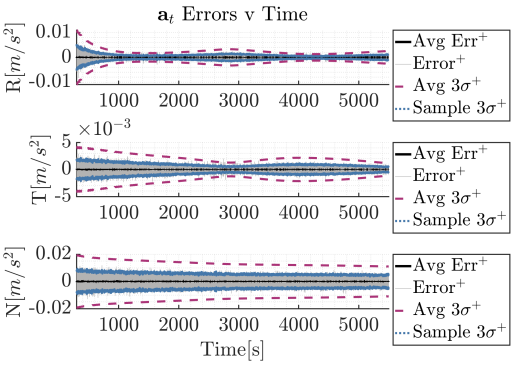

Figure 3: Unmodeled acceleration of the target vehicle errors in the target RTN frame versus time excluding initial 300s.

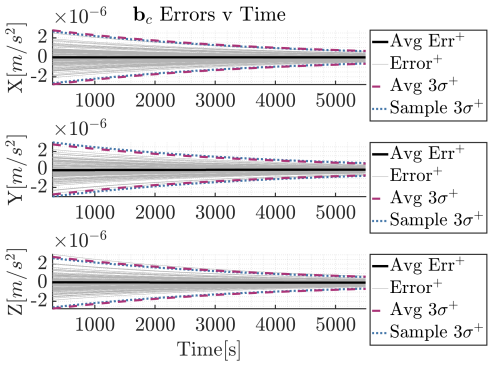

Figure 4: Chaser accelerometer bias errors in the chaser body frame versus time excluding initial 300s.

To further confirm that the filter is functioning properly, the posterior measurement residuals and their 3σ bounds are shown in Figures 5 and 6. Noticing that the measurement residuals appear to grow slightly as the scenario progresses in Figures 5 and 6. The adaptation takes this information in and in turn grows the process noise in the filter. This is a clear sign of the process noise adaptation at work. Examining the behavior in the latter half of the scenario in Figure 1, it is clear that the

errors would have grown outside of the estimated 3σ bounds as the scenario progressed without this adaptation.

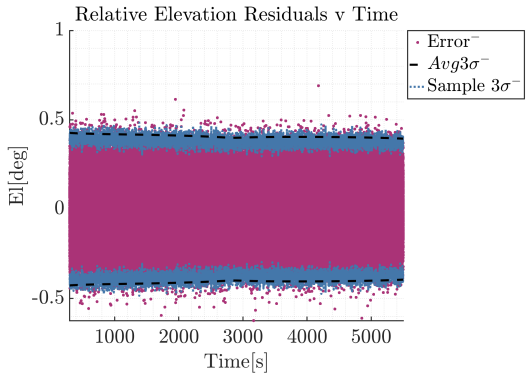

Figure 5: Elevation measurement residuals versus time excluding initial 300s.

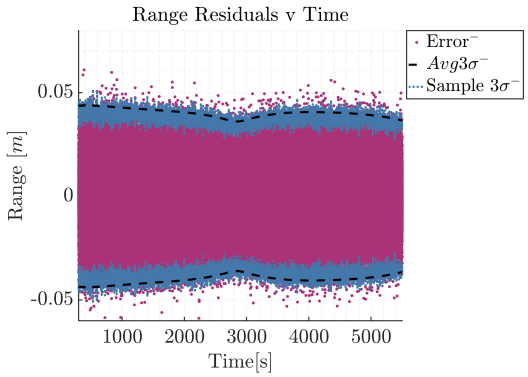

Figure 6: Range measurement residuals versus time excluding initial 300s.

CONCLUSIONS

This work demonstrates that correlation methods can be effectively utilized to enable a filter to autonomously adapt to unknown dynamics within a nonlinear, relative navigation scenario. Unlike prior studies where correlation methods were applied to linear systems, this research extends their application to environments with perturbations to a nonlinear system. The algorithm, referred to as MILTON, successfully recovers and maintains a well-bounded solution under these conditions. Historically, the positive definiteness of process noise in such studies has often been addressed heuristically. In contrast, other research has preserved definiteness using Riemann manifolds, albeit with significant computational expenses. In this work, positive definiteness is consistently maintained, and the information form of recursive least squares is utilized to mitigate the computational demands of the adaptation block, even with larger measurement buffers.

The growth of the space industry necessitates that future spaceflight vehicles enhance their ability to autonomously respond to a range of environmental variables. This includes addressing discrepancies within the onboard system model. If implemented, MILTON would empower vehicles in close proximity to effectively monitor each other and proactively respond to unmodeled perturbations. Such capabilities are essential for preventing collisions and ensuring successful rendezvous operations without the need for human intervention.

FUNDING SOURCES

This work was supported by a NASA Space Technology Graduate Research Opportunity, NASA grant number: 80NSSC22K1204.

REFERENCES

[1] R. E. Kalman, "A new approach to linear filtering and prediction problems," *Transactions of the ASME, Journal of Basic Engineering*, Vol. 82, No. 1, 1960, pp. 35–45.

[2] R. E. Kalman and R. S. Bucy, "New results in linear filtering and prediction theory," *Transactions of the ASME, Journal of Basic Engineering*, Vol. 83, No. 1, 1961, pp. 95–108.

[3] R. Mehra, "On the identification of variances and adaptive Kalman filtering," *IEEE Transactions on Automatic Control*, Vol. 15, No. 2, 1970, pp. 175–184.

[4] R. Mehra, "Approaches to adaptive filtering," *IEEE Transactions on Automatic Control*, Vol. 17, No. 5, 1972, pp. 693–698.

[5] P. R. Belanger, "Estimation of noise covariance matrices for a linear time-varying stochastic process," *Automatica*, Vol. 10, No. 3, 1974, pp. 267–275.

[6] J. Duník, O. Straka, and M. Šimandl, "On autocovariance least-squares method for noise covariance matrices estimation," *IEEE Transactions on Automatic Control*, Vol. 62, No. 2, 2016, pp. 967–972.

[7] B. J. Odelson, M. R. Rajamani, and J. B. Rawlings, "A new autocovariance least-squares method for estimating noise covariances," *Automatica*, Vol. 42, No. 2, 2006, pp. 303–308.

[8] B. M. Åkesson, J. B. Jørgensen, N. K. Poulsen, and S. B. Jørgensen, "A generalized autocovariance least-squares method for Kalman filter tuning," *Journal of Process Control*, Vol. 18, No. 7-8, 2008, pp. 769–779.

[9] J. Duník, O. Kost, and O. Straka, "Design of measurement difference autocovariance method for estimation of process and measurement noise covariances," *Automatica*, Vol. 90, 2018, pp. 16–24.

[10] R. Moghe, R. Zanetti, and M. R. Akella, "Adaptive Kalman Filter for Detectable Linear Time-Invariant Systems," *Journal of Guidance, Control, and Dynamics*, Vol. 42, No. 10, 2019, pp. 2197–2205, 10.2514/1.G004359.

[11] R. Moghe *et al.*, *Adaptive algorithms for identification of symmetric and positive definite matrices*. PhD thesis, 2021.

[12] A. P. Sage and G. W. Husa, "Adaptive filtering with unknown prior statistics," *Proceedings of the Joint Automatic Control Conference*, 1969, pp. 760–769.

[13] K. A. Myers and B. D. Tapley, "Adaptive sequential estimation with unknown noise statistics," *IEEE Transactions on Automatic Control*, Vol. 21, No. 4, 1976, pp. 520–523.

[14] M. R. Rajamani and J. B. Rawlings, "Estimation of the disturbance structure from data using semidefinite programming and optimal weighting," *Automatica*, Vol. 45, No. 1, 2009, pp. 142–148.

[15] N. Stacey and S. D'Amico, "Adaptive and dynamically constrained process noise estimation for orbit determination," *IEEE Transactions on Aerospace and Electronic Systems*, Vol. 57, No. 5, 2021, pp. 2920–2937.

[16] R. Moghe, R. Zanetti, and M. Akella, "Covariance Matching Kalman Filter for Observable LTI Systems," *2018 IEEE Conference on Decision and Control (CDC)*, IEEE, 2018, pp. 6372–6377.

[17] R. H. Shumway and D. S. Stoffer, "An approach to time series smoothing and forecasting using the EM algorithm," *Journal of Time Series Analysis*, Vol. 3, No. 4, 1982, pp. 253–264.

[18] P. Axelsson, U. Orguner, F. Gustafsson, and M. Norrlöf, "ML estimation of process noise variance in dynamic systems," *IFAC Proceedings Volumes*, Vol. 44, No. 1, 2011, pp. 5609–5614.

[19] R. L. Kashyap, "Maximum likelihood identification of stochastic linear systems," *IEEE Transactions on Automatic Control*, Vol. 15, No. 1, 1970, pp. 25–34.

[20] D. Lainiotis, "Optimal adaptive estimation: Structure and parameter adaption," *IEEE Transactions on Automatic Control*, Vol. 16, No. 2, 1971, pp. 160–170.

[21] C. Magnant, A. Giremus, E. Grivel, L. Ratton, and B. Joseph, "Bayesian non-parametric methods for dynamic state-noise covariance matrix estimation: Application to target tracking," *Signal Processing*, Vol. 127, 2016, pp. 135–150.

[22] Y. Huang, Y. Zhang, Z. Wu, N. Li, and J. Chambers, "A novel adaptive Kalman filter with inaccurate process and measurement noise covariance matrices," *IEEE Transactions on Automatic Control*, Vol. 63, No. 2, 2017, pp. 594–601.

[23] V. Mussot, G. Mercère, T. Dairay, V. Arvis, and J. Vayssettes, "Noise covariance matrix estimation with subspace model identification for Kalman filtering," *International Journal of Adaptive Control and Signal Processing*, 2021.

[24] L. Lennart, *System identification: Theory for the User*. Upper Saddle River, NJ, USA: Prentice-Hall, 1999.

[25] B. Schutz, B. Tapley, and G. H. Born, *Statistical orbit determination*. Elsevier, 2004.

[26] J. Duník, O. Straka, O. Kost, and J. Havlík, "Noise covariance matrices in state-space models: A survey and comparison of estimation methods-Part I," *International Journal of Adaptive Control and Signal Processing*, Vol. 31, No. 11, 2017, pp. 1505–1543.

[27] D. A. Vallado, *Fundamentals of astrodynamics and applications*, Vol. 12. Springer Science & Business Media, 2001.

[28] R. Zanetti and C. D'Souza, "Dual Accelerometer Usage Strategy for Onboard Space Navigation," *Journal of guidance, control, and dynamics*, Vol. 35, No. 6, 2012, pp. 1899–1902.

[29] D. Simon, *Optimal state estimation: Kalman, H infinity, and nonlinear approaches*. John Wiley & Sons, 2006.

[30] R. Zanetti, "Adaptable recursive update filter," *Journal of Guidance, Control, and Dynamics*, Vol. 38, No. 7, 2015, pp. 1295–1300.

[31] S. Servadio, R. Zanetti, and B. A. Jones, "Nonlinear filtering with a polynomial series of gaussian random variables," *IEEE Transactions on Aerospace and Electronic Systems*, Vol. 57, No. 1, 2020, pp. 647–658.

[32] C. Schmitt, T. Kämpfe, C. Kracht, K. Kanani, L. Scheunemann, R. Pforr, M. Windmüller, M. Schwarz, and M. Möller, "RVS 3000-X LiDAR – Applications From Docking to Sample Return and Lunar Landing," *46th Rocky Mountain AAS GNC Conference*, 2024.